ISSN 1392–1320 MATERIALS SCIENCE (MEDŽIAGOTYRA). Vol. 31, No. 4. 2025

Ultrasonic Processing Across Different Phases in Laser Welding of Large Thin-Walled Structures

Haodong LIU [1]*, Dongsheng WANG [2], Changjun CHEN [3], Aiyong CUI [1], Bing WANG [1], Li HAN [1]

[1] *Naval Aviation University Qingdao Branch, Qingdao Shandong 266041, China*
[2] *Wuxi Jinyan Laser Gas Turbine Parts Co., Ltd., Wuxi, Jiangsu 214429, China*
[3] *School of Mechanical and Electric Engineering, Soochow University, Suzhou, Jiangsu 215021, China*

http://doi.org/10.5755/j02.ms.39720

Received 9 December 2024; accepted 5 February 2025

In laser welding applications for large structures like oil storage tanks, ships, automobiles, and high-speed rail, effective post-weld heat treatment is challenging because the structures are large and cannot be disassembled. This results in significant residual welding stress, leading to reduced mechanical properties, shorter fatigue life, and excessive welding deformation, which compromises assembly accuracy. Current studies on ultrasonic field application in thin-walled structures predominantly position the ultrasonic source directly beneath the welding pool. While this approach offers high ultrasonic transfer efficiency and a straightforward physical model, it is impractical for large, enclosed, or non-transparent structures, where access from behind is limited and weld protection is required. This paper proposes a novel process model that positions the ultrasonic source on the same side as the welding pool, addressing key challenges in practical engineering. Preliminary investigations into critical aspects of this model provide a foundation for further research and potential industrial application.

Keywords: laser welding, ultrasonic field, welding morphology, micro-structure.

1. INTRODUCTION

After years of development, laser welding technology has matured and is now widely used in industrial fields such as aerospace, automotive manufacturing, high-speed rail, shipbuilding, and the petroleum and petrochemical industries, owing to its advantages. These include a small heat-affected zone, consistent quality, minimal welding deformation, high automation potential, and the ability to weld challenging materials [1 – 5]. However, the localized high-power density heat input during laser welding generates a steep temperature gradient, resulting in uneven thermodynamic effects. Combined with rapid solidification and the constraints of the weld pool and base material, this leads to the formation of residual stress.

Additionally, laser welding, characterized by rapid heating and cooling, often results in high cooling rates and significant temperature gradients, which contribute to uneven weld joint structures and defects such as porosity. Residual stress, structural segregation, and porosity are the three primary factors that reduce the service life of welded structures. For large, thin-walled structures such as aircraft components, oil storage tanks, ships, automobiles, and high-speed rail cars, post-weld heat treatment is often impractical due to the size and non-disassembly nature of these structures. Consequently, significant residual stress accumulates at the weld site, leading to diminished mechanical performance and reduced service life [6, 7]. Furthermore, substantial welding deformation compromises assembly accuracy, which severely restricts advancements in equipment manufacturing and maintenance capabilities in China.

Numerous studies have explored the introduction of auxiliary ultrasonic fields during laser welding to improve microstructure and reduce residual stress and defects. A common approach involves applying the ultrasonic field directly beneath the weld pool, as illustrated in Fig. 1. This method offers high efficiency in ultrasonic energy transfer and a straightforward physical model. However, in practical engineering applications, thin-walled structures often present challenges due to their large volume, near-enclosed design, restricted internal space, and opacity [8 – 10], as shown in Fig. 2. Moreover, certain welding processes require weld seam protection on the backside, making it difficult to position ultrasonic sources beneath the weld pool or inside the structure. As a result, existing methods of introducing ultrasonic fields are unsuitable for welding large thin-walled structures in real-world applications.

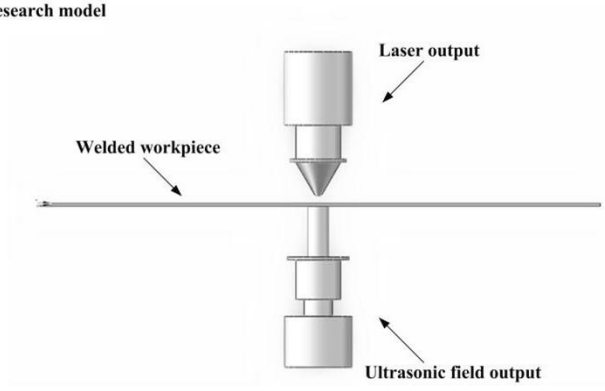

Fig. 1. Schematic of the traditional research model

* Corresponding author: H.D. Liu
E-mail: *mdlhd@sina.com*

Given these limitations, it is crucial to develop in-situ welding treatment technologies tailored to large thin-walled structures such as aircraft bulkheads, oil storage tanks, ship components, automotive frames, and high-speed rail carriages. Advancing these technologies can significantly enhance welding quality and the durability of welded structures. Moreover, this research holds substantial engineering and economic value, particularly in elevating China's equipment manufacturing and maintenance standards.

a

b

c

Fig. 2. Typical large-size and thin-wall welded construction: a – large oil storage tanks; b – high-speed train carriages; c – ship structures

2. A MODEL FOR ULTRASONIC PROCESSING ACROSS DIFFERENT PHASES BASED ON LASER WELDING

The fundamental principle of ultrasonic processing across different phases in laser welding is to regulate the unstable deformation and microstructural properties of laser-welded repair joints by introducing an ultrasonic field in the near-weld zone during the welding process. This approach primarily involves three key action processes:

1. During the laser welding process, the ultrasonic field interacts with the workpiece as it undergoes phase transitions from solid to liquid and back to solid. This interaction influences the structural morphology, grain size, and orientation, effectively reducing residual stress and minimizing welding defects.
2. The ultrasonic field acts on the high-temperature superplastic stage of solidified welds. The primary factors influencing hot deformation include deformation temperature, strain rate, and deformation magnitude, with deformation temperature and strain rate having the most significant impact, as described in Eq. 1 [11]:

$$\sigma = \sigma_0 e^{\left(-bT/T_0+b_2\right)}\left(\frac{\varepsilon}{\varepsilon_0}\right)^{b_3}\left(\frac{\dot{\varepsilon}}{\dot{\varepsilon}_0}\right)^{\left(b_4+b_5T/T_0\right)}, \quad (1)$$

Where σ is the deformation resistance; σ_0 is the base value of deformation resistance; T is the temperature of deformation; $\dot{\varepsilon}$ is the rate of deformation; $\dot{\varepsilon}_0$ is the base value of the rate of deformation; ε is the degree of deformation; ε_0 is the base value of the degree of deformation; $b_1 \sim b_5$ are regression coefficients. It can be observed that the deformation resistance of a material decreases with increasing temperature. Consequently, high-temperature welds exhibit lower resistance to plastic deformation and creep, making it easier to achieve small plastic elongation and reduce internal deformation irregularities under the influence of an ultrasonic field.

3. The aging effect of the ultrasonic field on weld seams. The superposition of the ultrasonic field and the residual stress field can cause localized, instantaneous stress in the welded structure to reach or exceed its yield strength. This results in plastic deformation and the release of residual stress. Even when the combined stress does not reach the material's yield strength, residual stress can still be alleviated through dislocation movement in the joint, producing micro-plastic deformation.

The ultrasonic processing model for laser welding proposed in this study positions the ultrasonic vibration source near the same side of the molten pool (as shown in Fig. 3). This configuration enables convenient and efficient welding of large-sized or nearly enclosed shell structures. However, changes in the ultrasonic input method (direction and position) fundamentally alter the theoretical process model, significantly increasing research complexity in two major areas:

1. Reduced input efficiency: unlike direct ultrasonic input from beneath the molten pool, the same-side input method results in significantly lower energy transfer efficiency. To compensate, ultrasonic field power must be substantially increased. Preliminary studies indicate that this shift raises the required power from approximately 300 W to over 1500 W. The potential impact of high-power ultrasonic waves on the directly affected regions of the welded structure, including risks of impact damage and fatigue, necessitates further investigation and optimization.
2. Complexity of the theoretical model: the theoretical model for ultrasonic input welding assumes thin-plate fixed-support vibration in the context of mechanical vibration.

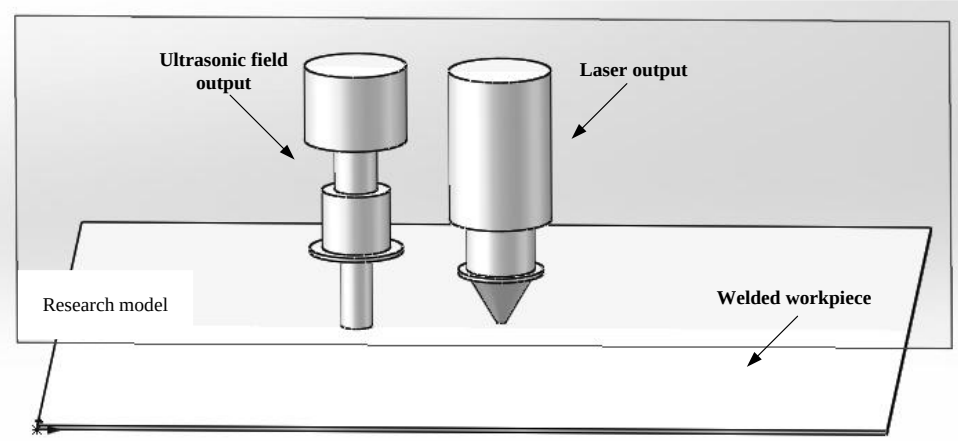

Fig. 3. Schematic of the research model presented in this paper

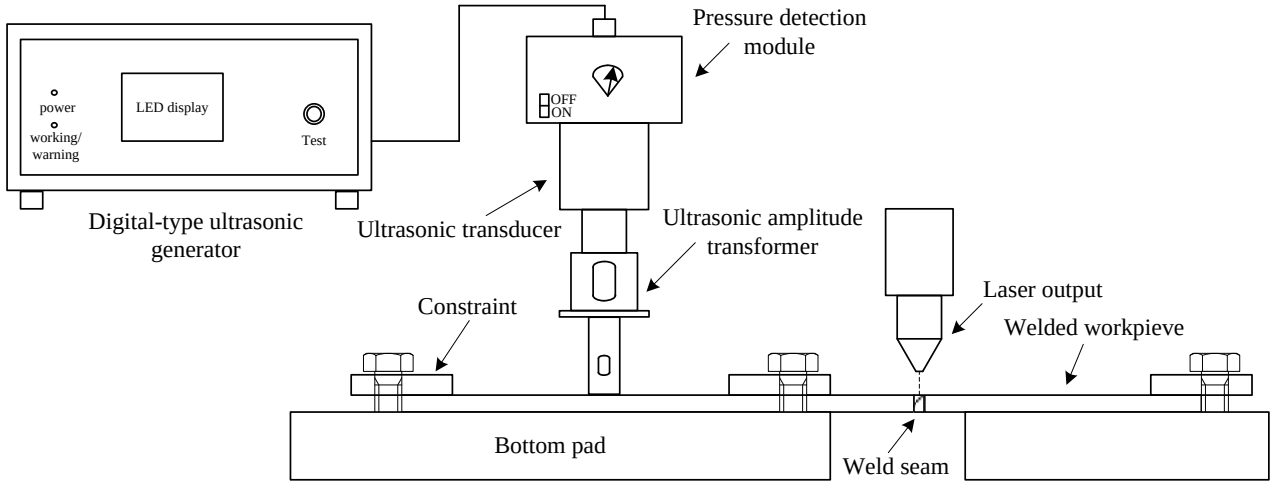

Fig. 4. Schematic of welding processing with ultrasonic system

This model involves complex couplings between the ultrasonic field, molten pool flow field, stress field, and temperature field. Shifting the ultrasonic field source from directly beneath the molten pool to a nearby position, as proposed, reduces physical constraints but significantly increases the complexity of the theoretical model.

3. EXPERIMENTAL SETUP

Based on the research model and laboratory experiments, the ultrasonic processing system for different phases in laser welding was constructed, as illustrated in Fig. 4. The system primarily comprises a workbench, welding robot, laser, ultrasonic vibration system, and other components. The system layout is designed to closely replicate the actual conditions of laser welding large-sized thin-walled structures within near-enclosed shells. Under real-world welding conditions, the welded section is integrated with the entire structure and behaves as a unified whole. However, significant disparities in mass and volume exist between the welding area and the overall structure. Consequently, the design and research of the model emphasize fully constraining the thin plate welding structure.

To begin, a test piece with simulated cracks is secured onto the welding workbench using hexagonal fastening bolts and pressure blocks. A torque wrench is then used to apply a specific pre-tightening force (as shown in Fig. 5), ensuring that the ultrasonic vibration aligns with the welding heat source's direction. For experimental simplicity, both the ultrasonic vibration and welding heat source inputs are set to act vertically downward, without compromising the research outcomes. The structure to be welded is positioned horizontally to facilitate the process [12].

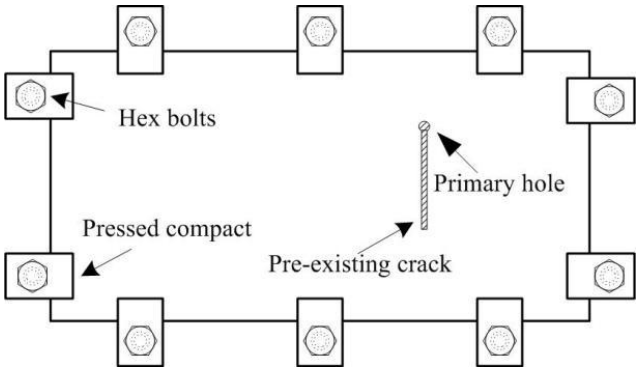

Fig. 5. Schematic of full restraining experiment structure

4. FEASIBILITY VALIDATION OF THE PROCESS

The material used for the verification test is annealed TC4 titanium alloy, and the material composition is shown in Table 1.

The YAG pulse-type laser welding machine, where the ERCR-HP3-AA00 robot was the actuator, was used. The laser welding process parameters are shown in Table 2, and the workpiece was polished and cleaned with acetone before welding.

Table 1. Chemical compositions of TC4, wt.%

Al	V	Fe	O	H	Ti
6.15	4.13	0.08	0.009	0.002	Allowance

Table 2. Laser welding parameters

Current *C*, A	Pulse width *I*, ms	Frequency *f*, Hz	Welding speed *v*, mm·s^{-1}	Spot diameter *D*, mm
175	9	6	2	0.3

In the verification test, a stepped deformation amplitude rod tool head is used to apply an ultrasonic vibration field to the fully constrained test piece. The center of the ultrasonic field is positioned 100 mm away from the molten pool, with the weight of the vibration head serving as the downward pressure in the normal direction.

4.1. Influence of ultrasonic cross-phase processing on the macroscopic morphology of weld seams

The surface contour of the laser welding molten pool without additional ultrasonic field and with an applied power of 1200 W ultrasonic field are shown in Fig. 6 a and b respectively. The results were measured by VEECO WYKO NT1100 type non-contact three-dimensional surface morphology instrument, the scanning area is 2.5 mm × 1.5 mm, the measurement area was the weld joint and its vicinity, finally the measurement work was completed by using system software.

Surface roughness indicates the macroscopic morphology of the weld seam, reflects the micro-geometric features of peaks and valleys with small intervals on the surface [13]. The roughness can be quantified by the height gradient difference.

It was observed that the maximum height gradient difference for a conventional laser weld seam with a single pulse is 62 μm, while for a laser weld seam with an added ultrasonic field, the maximum height gradient difference decreases to 59 μm. As such, the surface roughness of the laser weld seam with an ultrasonic field is lower than that of the conventional laser weld seam. Increased surface roughness can lead to stress concentration at the weld joint, which reduces the fatigue strength. Therefore, it can be inferred that the fatigue resistance of laser welds treated with ultrasonic cross-phase processing is superior to that of conventional welds [14].

4.2. Influence of ultrasonic cross-phase processing on the microstructure morphology of weld seams

This article primarily employs the three-circle intercept method to measure the microstructural grain size of laser weld joints [15].

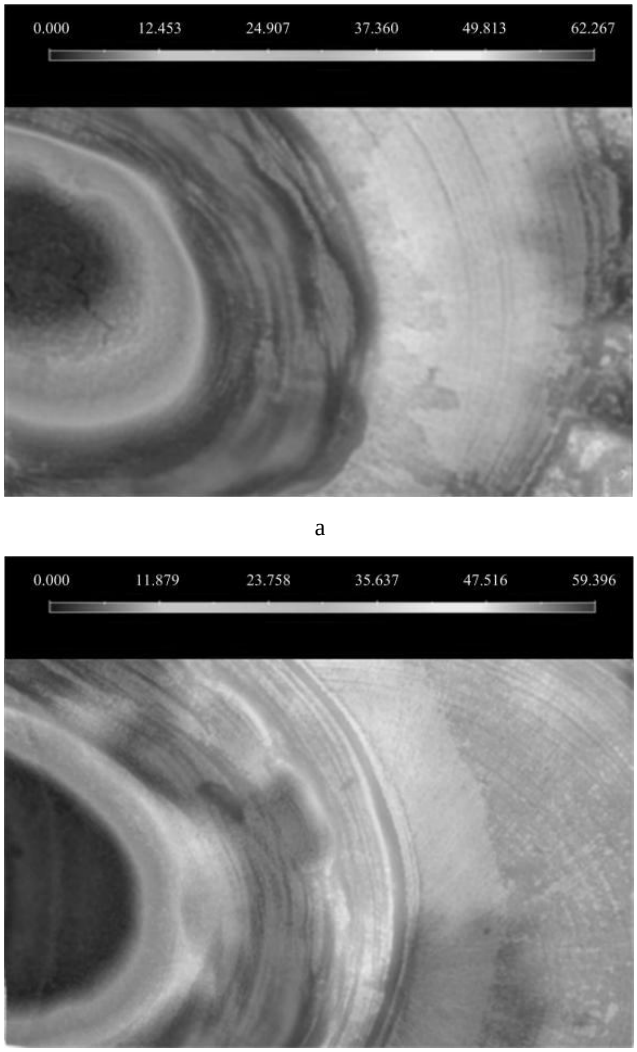

Fig. 6. Profile morphology of laser welding joints surface: a – without ultrasonic vibration field; b – 1200 W

The tissue was observed by using the KH-7700 three-dimensional video microscope system, Fig. 7 and Fig. 8 present metallographic images of the conventional laser weld joint and the laser weld joint under various ultrasonic field power conditions, captured at 350× magnification using an optical microscope (OM). The grain size measurement diagrams were processed using SRMAS software [16].

Fig. 7. Grain size without ultrasonic vibration

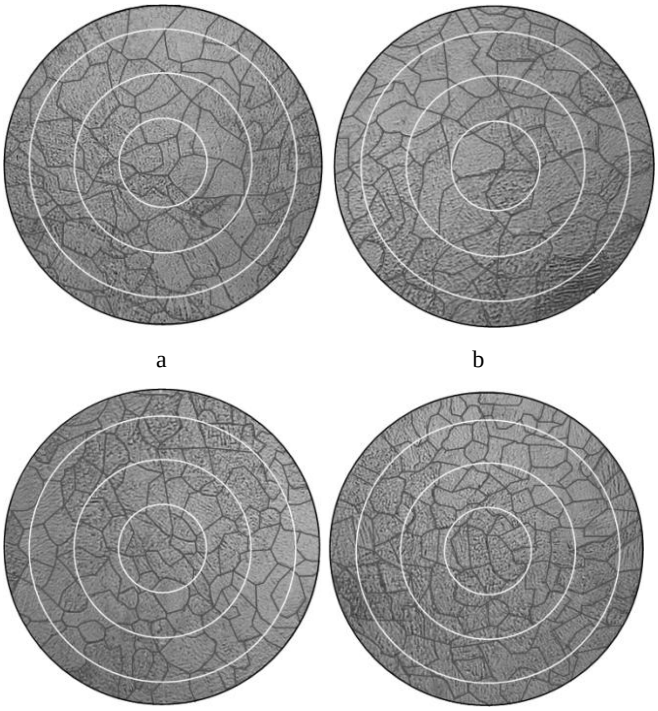

Fig. 8. Grain size in different ultrasonic vibration power: a – 400 W; b – 800 W; c – 1200 W; d – 1600 W

Related studies [17] have indicated that when the total number of cutoff points for the same sample across different fields approaches 500, the accuracy becomes relatively reliable. Therefore, this article selects six measurement fields. Table 3 below presents the cutoff points for samples in different experimental groups across the six selected fields.

Table 3. Section number statistics

Field / Power	F_1	F_2	F_3	F_4	F_5	F_6
0 W	58	61	65	61	62	64
400 W	67	70	73	74	71	73
800 W	83	78	81	79	80	82
1200 W	85	88	86	89	88	90
1600 W	95	91	93	93	92	97

A normality test conducted on the data in the table reveals that the cutoff numbers for each experimental group in different fields follow a normal distribution. Therefore, statistical methods based on normal distribution can be applied for further analysis. As a result, data such as grain size levels, confidence intervals, and relative errors for the different experimental groups are presented in Table 4, where $\bar{F}$ is the average number of truncations, S is the standard deviation, G is the mean grain size, 95 % CI is the corresponding confidence interval of G, % RA is the relative error. As shown in Table 4, with the increase of ultrasonic field power, the grain size of the joint tissue gradually decreases, and there is a well-known Hall-Petch relationship between the grain size of the joint tissue and the weld seam performance [18].

$$\sigma_{el} = \sigma_0 + k_0 \delta^{-\frac{1}{2}}, \quad (2)$$

where δ represents grain size; σ_{el} represents yield strength; σ_0 and k_0 are constants.

Table 4. Statistical samples

Variable / Power	$\bar{F}$	S	G	95% CI	G±95%	%RA
0 W	61.8	2.48	7.58	0.12	7.58±0.12	1.60%
400 W	71.3	2.58	7.99	0.11	7.99±0.11	1.38%
800 W	80.5	1.87	8.34	0.07	8.34±0.07	0.84%
1200 W	87.7	1.86	8.59	0.06	8.59±0.06	0.70%
1600 W	93.5	2.17	8.78	0.07	8.78±0.07	0.80%

Therefore, it can be observed that as the grain size of the joint structure decreases, the strength and hardness of the weld seam increase significantly, while the plasticity and toughness of the joint are also notably improved.

5. DESIGN OF ULTRASONIC PROCESSING ACROSS DIFFERENT PHASES BASED ON LASER WELDING DEVICE

Based on the research model described above, combined with practical experience in laser welding external fields and using an integrated approach, a field ultrasonic processing system for different phases based on laser welding is designed for large thin-walled structures, as shown in Fig. 9 and Fig. 10.

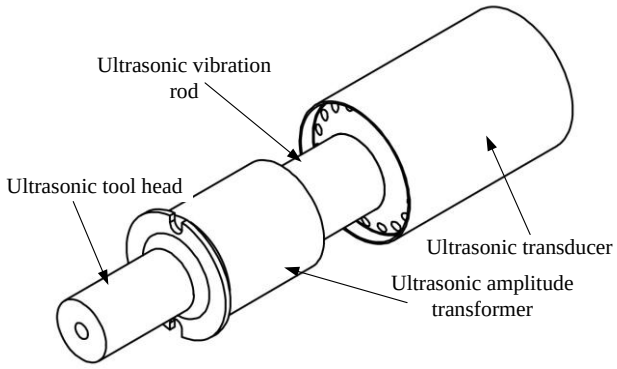

Fig. 9. 3D modeling of ultrasonic vibrator

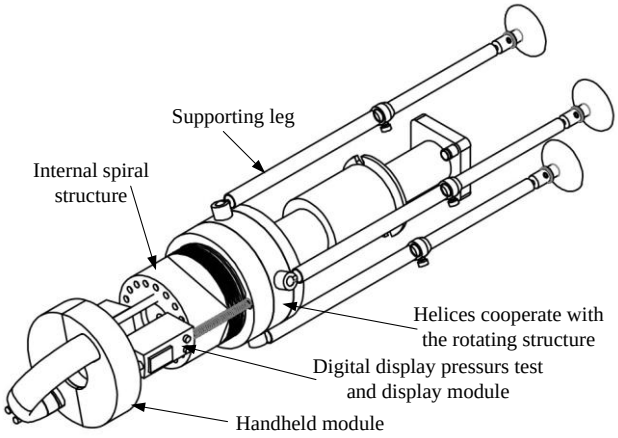

Fig. 10. 3D modeling of auxiliary structure

This equipment is designed for easy single-person portability and is suitable for ultrasonic cross-phase processing of large thin-walled structures in various positions and orientations. The ultrasonic vibrator, which

implements the cross-phase processing technology, consists primarily of an ultrasonic transducer and an ultrasonic amplitude rod. Its auxiliary components include support legs, a threaded rotating mechanism, an internal screw mechanism, a digital pressure testing and display system, and an armrest cover.

6. CONCLUSIONS

1. The process control of laser welding repair joints, focusing on instability and microstructure performance, involves three key action stages: the phase change process of the weld seam during laser welding, the high temperature superplasticity stage of the solidified weld seam, and the aging process of the weld seam after welding.
2. The ultrasonic processing system, based on laser welding, is designed to simulate the actual construction conditions for laser welding large thin-walled structures with near-closed shells. In this setup, the welded parts are integrated with the entire structure and function as a unified whole, while the welding area exhibits significant differences in physical properties (such as quality and volume) compared to the overall structure.
3. Feasibility verification tests demonstrate that the ultrasonic processing across different phases based on the laser welding process can significantly reduce the surface roughness of laser welds and the size of microstructural grains, thereby improving the overall performance of the welds.
4. The designed portable ultrasonic processing device, based on laser welding, allows for easy single-person operation and is suitable for laser welding of large thin-walled structures at various positions and orientations. This device is particularly useful for in-situ external field laser welding applications for repairing large thin-walled structure damage.

Acknowledgments

This work was supported by the Shandong Provincial Natural Science Foundation (Grant number [ZR2022ME217]).

REFERENCES

1. **Xia, L., Kang, Y., Yu, H.S., Wu, Y.F., Zhan, X.H.** Equiaxed Grains in Laser Welded 2060 Al-Li Alloys and Their Formation Mechanism *Chinese Journal of Laser* 45 (11) 2018: pp. 1102013. https://doi.org/10.3788/CJL201845.1102013
2. **Luo, B.B., Zhang, H., Lei, M., Feng, Y., Xu, L.F., Liu, D.J.** Laser Welded Joints of Automotive 6016 Aluminum and Low Carbon Steel: Interface Microstructure and Mechanical Properties *Materials Reports* 34 (2) 2020: pp. 04108 – 04112. https://doi.org/10.11896/cldb.19020085
3. **Li, F.Q., Li, M.W., Meng, X.X.** Effect of Heat Treatment on Microstructure and Property of 6005A Aluminum Alloy Laser Welding Joint *Materials Science and Technology* 29 (2) 2021: pp. 44 – 50. https://doi.org/10.11951/j.issn.1005-0299.20200253
4. **Yu, H., Li, R.F., Liu, H.Y., Qi, K., Liu, B.** Research on Laser Welding of Light Alloy Structure for Naval Ship *Ship Science and Technology* 42 (3) 2020: pp. 47 – 51. https://doi.org/10.3404/j.issn.1672-7649.2020.03.010
5. **Liang, Z.Z., Zhang, H.T., Zhang, L.P.** Damage Analysis and Repair of Blade of Circulating Gas Compressor in Acrylic Acid Plant *Petro-Chemical Equipment* 49 (3) 2020: pp. 76 – 80. https://doi.org/10.3969/j.issn.1000-7466.2020.03.013
6. **Li, Y.C., Chen, D.F., Zu, Y., Liu, X.L., Li, M.J., Bai, R.Y., Hou, Y.H., Li, Y.Q., Sun, K.** Effect of Post Weld Heat Treatment on Microstructure and Residual Stress in 16MND5 Steel Welded Joint *Atomic Energy Science and Technology* 55 (10) 2021: pp. 1850 – 1856. https://doi.org/10.7538/yzk.2020.youxian.0782
7. **Luo, J.Y., Zhang, Y.X., Lü, C.K.** Numerical Smulation of the Effect of Post-Welding Heat Treatment on Fatigue Life of Titanium Alloy Butt Plate *Iron Steel Vanadium Titanium* 44 (5) 2023: pp. 76 – 83. https://doi.org/10.7513/j.issn.1004-7638.2023.05.012
8. **Wang, T.** Analysis and Control of Welding Deformation of Steel Storage Tank *Total Corrosion Control* 35 (2) 2021: pp. 85 – 86, 9. https://doi.org/10.13726/j.cnki.11-2706/tq.2021.02.085.02
9. **Guo, W.W., Huang, J.Q., Xue, L., Huang, J.F., Han, F.** Numerical Simulation of Deformation with Welding Aluminum Alloy Profile of Side Wall of High-speed Train *Journal of Beijing Institute of Petrochemical Technology* 28 (3) 2020: pp. 37 – 42. https://doi.org/10.19770/j.cnki.issn.1008-2565.2020.03.008
10. **Zhao, J.** Study on the Affections of Residual Stress in the Hull Structure Welding and the Ways of Stress Releasing *Wireless Internet Technology* 17 (1) 2020: pp. 139 – 140. https://doi.org/10.3969/j.issn.1672-6944.2020.01.063
11. **Qi, Y.W., Chen, H.R., Wang, X.H., Xie, H.Z., Fu, H.G., Zhao, T.Z.** High Temperature Deformation Behavior and Damage Mechanism of TC4 Titanium Alloy *Ordnance Material Science and Engineering* 47 (4) 2024: pp. 8 – 14. https://doi.org/10.14024/j.cnki.1004-244x.20240528.002
12. **Sui, C.F., Liu, Z.J., Ai, X.Y.** Effect of Ultrasonic Vibration on Welding Hot Crack of 6061 Aluminum Alloy *Transactions of the China Welding Institution* 44 (1) 2023: pp. 122 – 128. https://doi.org/10.12073/j.hjxb.20220106002
13. **Lv, G.Y., Zhu, Y.L., Li, L., Han, X.G.** The Effect of Ultrasonic Deep Rolling (UDR) on Surface Topography and Surface Roughness of TC4 Titanium Alloy *China Surface Engineering* 20 (4) 2007: pp. 38 – 41. https://doi.org/10.3321/j.issn:1007-9289.2007.04.008
14. **Dong, D.K., Chen, A., Li, X.F., Zhang, H.Y.** Effect of Surface Roughness on Fatigue Property of TC4 Titanium Alloy by Selective Laser Melting *Journal of Mechanical Strength* 42 (5) 2020: pp. 1094 – 1098. https://doi.org/10.16579/j.issn.1001.9669.2020.05.012
15. **Yu, C.F., Hsieh, K.C.** The Mechanism of Residual Stress Relief for Various Tin Grain Structures *Journal of Electronic Materials* 39 (8) 2010: pp. 1315 – 1318. https://doi.org/10.1007/s11664-010-1289-y
16. **Liu, H.D., Hu, F.Y., Cui, A.Y., Dai, J.T., Huang, F., Li, H.B.** Effect of Ultrasonic Vibration on Grain Size of TC4 Titanium Alloy Laser Welding Joints *Chinese Journal of Laser* 43 (8) 2016: pp. 0802005. https://doi.org/10.3788/CJL201643.0802005
17. **Wu, J., Yang, R.G., Zhou, Z.C., Lei, N., Zhao, N.S., Yang, Y.L., Zhang, H.Y., Xie, X.Y., Shen, J., Wang, M.H.**

Comparison of Results from Different Grain Size Measurement Methods *Physical Testing and Chemical Analysis Part A:Physical Testing* 60 (3) 2024: pp. 23 – 26. https://doi.org/10.11973/lhjy-wl202403006

18. **Wang, Y., Wang, Y.T., Li, R.D., Niu, P.D., Wang, M.B., Yuan, T.C., Li, K.** Hall-Petch Relationship in Selective Laser Melting Additively Manufactured Metals: Using Grain or Cell Size *Journal of Central South University* 28 (4) 2021: pp. 1043 – 1057. https://doi.org/10.1007/s11771-021-4678-X